Available online at www.sciencedirect.com
SCIENCE DIRECT®
Nuclear Instruments and Methods in Physics Research A 531 (2004) 428–434
NUCLEAR INSTRUMENTS & METHODS IN PHYSICS RESEARCH Section A
www.elsevier.com/locate/nima

Recoil separator ERNA: charge state distribution, target density, beam heating, and longitudinal acceptance ☆

D. Schürmann[a], F. Strieder[a], A. Di Leva[a,b], L. Gialanella[b], N. De Cesare[c], A. D'Onofrio[d], G. Imbriani[b], J. Klug[a], C. Lubritto[d], A. Ordine[b], V. Roca[b], H. Röcken[a], C. Rolfs[a,*], D. Rogalla[d], M. Romano[b], F. Schümann[a], F. Terrasi[d], H.P. Trautvetter[a]

[a] *Institut für Physik mit Ionenstrahlen, Ruhr-Universität Bochum, Experimentalphysik III, Bochum 44801, Germany*
[b] *Dipartimento di Scienze Fisiche, Università Federico II, Napoli and INFN, Napoli, Italy*
[c] *Dipartimento di Scienze della Vita, Seconda Università di Napoli, Caserta and INFN, Napoli, Italy*
[d] *Dipartimento di Scienze Ambientali, Seconda Università di Napoli, Caserta and INFN, Napoli, Italy*

Accepted 18 May 2004

Available online 23 July 2004

Abstract

For improved cross section measurements of the reaction $^{12}C(\alpha,\gamma)^{16}O$ in inverted kinematics, a recoil separator ERNA is developed at the 4 MV Dynamitron tandem accelerator in Bochum to detect directly the ^{16}O recoils with high efficiency. The ^{16}O recoils are produced by the ^{12}C projectiles in a windowless ^{4}He gas target. We report on the charge state distribution of the ^{16}O recoils, the gas target density, the beam heating of the gas target, and the acceptance of the separator along the extended gas target.

Keywords: Recoil separator

1. Introduction

The reaction $^{12}C(\alpha,\gamma)^{16}O$ ($Q = 7.16\,MeV$) takes place during helium burning in Red Giants [1]. The cross section at the relevant Gamow-energy, $E_o = 0.3\,MeV$, determines—together with the convection mechanism in the helium stellar core— the abundances of carbon and oxygen at the end of helium burning. This in turn influences the

☆ Supported in part by Deutsche Forschungsgemeinschaft (Ro429/35-2) and Istituto Nazionale di Fisica Nucleare (INFN).
* Corresponding author. Fax: 0049-234-32-14172.
E-mail address: rolfs@ep3.ruhr-uni-bochum.de (C. Rolfs).

0168-9002/$ - see front matter © 2004 Elsevier B.V. All rights reserved.
doi:10.1016/j.nima.2004.05.131

nucleosynthesis of elements up to the iron region for massive stars [2] and the composition of C/O white dwarfs in the case of intermediate mass stars [3]. For these reasons, the cross section $\sigma(E_o)$ should be known with a precision of at least 10%. In spite of experimental efforts over nearly 30 years [4–12], one is still far from this goal. All previous efforts have focused on the observation of the capture γ-rays, including one experiment [7] that combined γ-detection with coincident detection of the ^{16}O recoils. Due to the low cross section and various backgrounds depending on the exact nature of the experiments, γ-ray data with useful, but still inadequate, precision were limited to center-of-mass energies $1.2\,\mathrm{MeV} \leqslant E_{cm} \equiv E \leqslant 3.2\,\mathrm{MeV}$.

To improve the situation, a new experimental approach has been undertaken at the 4 MV Dynamitron tandem accelerator in Bochum, called ERNA = European Recoil Separator for Nuclear Astrophysics [13–16]. In this approach, the reaction is initiated in inverted kinematics, $^4He(^{12}C,\gamma)^{16}O$, i.e. a ^{12}C ion beam is guided into a windowless ^4He gas target and the ^{16}O recoils are counted in a ΔE-E telescope placed in the beam line at the end of the separator, where the separator filters the intense ^{12}C projectiles from the ^{16}O recoils. ERNA is designed to study the reaction over the energy range $E = 0.7$ to 5.0 MeV. In the present work we report on the charge state distribution of the ^{16}O recoils, the gas target density, the beam heating of the gas target, and the acceptance of the separator along the extended gas target.

2. ERNA setup

The ERNA setup (Fig. 1) has been described previously [13–16]. Briefly, the ion beam emerging from the tandem is focused by a quadrupole doublet (QD1), filtered by a 52° analysing magnet, and guided into the 75° beam line of ERNA by a switching magnet (these elements are not shown in Fig. 1). A quadrupole doublet (QD2) after the switching magnet is used to focus the beam on the gas target. For the purpose of beam purification, there is one Wien filter (WF1) before the analysing magnet and one (WF2) between QD2 and the gas target. For the simulation of the angular spread of the ^{16}O recoils, there is a quadrupole doublet (QD3) shortly before the gas target. After the gas target, the separator consists sequentially of the following elements: a quadrupole triplet (QT), a Wien filter (WF3), a quadrupole singlet (QS1), a 60° dipole magnet, a quadrupole doublet (QD4), a Wien filter (WF4), and the ΔE-E telescope. Finally, several steerers (ST), Faraday cups (FC), slit systems (SS), and apertures (AP) are installed along the beam line for setting-up and monitoring purposes.

3. Charge state distribution of ^{16}O recoils in ^4He gas

In a recoil separator such as ERNA that includes analysis of magnetic rigidity, one makes a charge state selection of the recoils, causing a reduction in the number of recoils transmitted through the separator. However, since there is

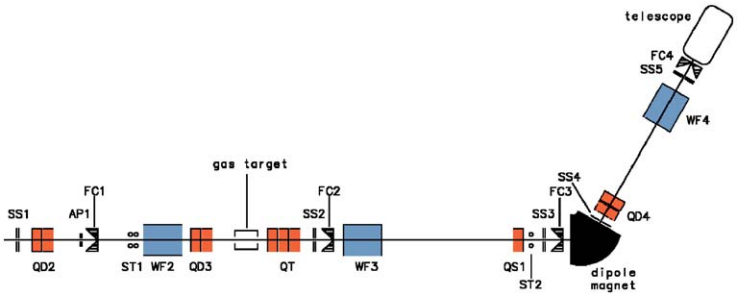

Fig. 1. Schematic diagram of the recoil separator ERNA: WF = Wien filter, QS = quadrupole singlet, QD = quadrupole doublet, QT = quadrupole triplet, ST = steerer, FC = Faraday cup, SS = slit system, AP = aperture. At the end of the separator, there is a ΔE-E telescope for particle identification.

usually—in the equilibrium charge state distribution—a charge state representing about 50% of the total recoils produced, this reduction is not serious. Since the ^{16}O recoils are produced in the ^{4}He gas target, their charge state distribution depends however on the geometric location within the target: those ^{16}O recoils produced in the upstream part of the target will most likely reach an equilibrium charge state distribution in the passage of the remaining target length, while those ^{16}O recoils produced near the downstream end of the target will not. Thus, not all ^{16}O recoils produced will be characterized by an equilibrium charge state distribution and this feature can lead to significant uncertainties in the cross section determination.

The charge state distribution of ^{16}O ions in ^{4}He gas was measured as a function of gas pressure: for each charge state the separator was set properly and the resulting current observed at the end of the separator in FC4 (Fig. 1). The results obtained at $E_{\mathrm{lab}} = 9.6\,\mathrm{MeV}$ are shown in Fig. 2 for an incoming charge state $q_{\mathrm{in}} = 3^{+}$. Similar results were obtained for other incoming charge states of the ^{16}O ions ($q_{\mathrm{in}} = 4^{+}$ to 6^{+}) as well as for ^{12}C ions of different incoming charge states at the corresponding energy $E_{\mathrm{lab}} = 12.8\,\mathrm{MeV}$. In order to arrive at the charge state distribution of the ^{16}O recoils from $^{4}\mathrm{He}(^{12}\mathrm{C},\gamma)^{16}\mathrm{O}$, we integrated these curves from zero pressure to a chosen pressure, where we assumed a charge state conservation in the transition from the ^{12}C ions to the ^{16}O recoils. In the integration we included at each differential length of the gas target cell the charge state distribution of the incoming ^{12}C ions as well as the charge state change of the ^{16}O ions over the remaining gas target length. The procedure simulates and includes the different geometrical locations of the ^{16}O recoils. The resulting curve for the 6^{+} charge state of the ^{16}O recoils is shown in Fig. 3. The results are compared (Fig. 3) with the 6^{+} charge state probabilities as a function of ^{4}He pressure, which were measured for $^{4}\mathrm{He}(^{12}\mathrm{C},\gamma)^{16}\mathrm{O}$ (with a $^{12}\mathrm{C}^{3+}$ incoming ion beam) using the telescope at the end of the separator: here the observed yields ^{16}O were normalized to the rates observed with the post-stripper Ar gas (Section 4). One observes a clear discrepancy between calculation and observation indicating that the above assumption does not represent the (unknown) charge state transfer mechanisms between the ^{12}C ions and the ^{16}O recoils.

4. Charge state distribution of ^{16}O recoils in an Ar post-stripper

To remove the above uncertainties, a post-stripper of sufficient thickness was installed after the ^{4}He gas target. In the first step, we used a

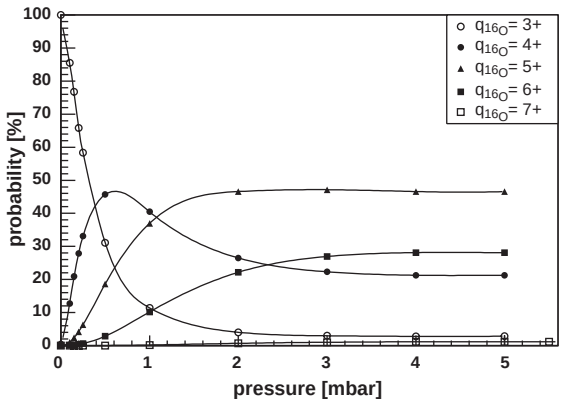

Fig. 2. Charge state distribution of ^{16}O ions ($q_{\mathrm{in}} = 3^{+}, E_{\mathrm{lab}} = 9.6\,\mathrm{MeV}$) in ^{4}He gas as a function of ^{4}He pressure in the gas target cell. The curves through the data points are to guide the eye.

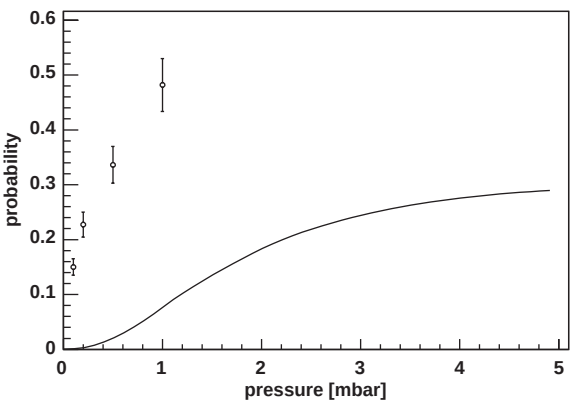

Fig. 3. Calculated 6^{+} charge state probability of ^{16}O recoils as a function of ^{4}He gas pressure (solid curve) is compared with observation (data points).

$4\,\mu g/cm^2$ thick C foil (obtained from the Technische Universität München). However, the foil broke after about 3 hours of ^{12}C beam bombardment (5 pμA) and more troublesome—we observed a high rate of ^{16}O nuclides in the telescope due to the $^{12}C(^{12}C, ^{8}Be)^{16}O$ and $^{12}C(^{12}C, \alpha\alpha)^{16}O$ reactions initiated in the foil; the reactions are known to have a cross section at the relevant ^{12}C energies [17] about 2–3 orders of magnitude higher than that of $^{4}He(^{12}C, \gamma)^{16}O$. Thus, a C foil was not an acceptable solution. Instead, we installed a gaseous post-stripper after the primary ^{4}He gas target consisting of a cell of 30 mm length and apertures of 13 mm diameter (33 mm distance between the exit of the gas target cell and the entrance of the post-stripper cell). As stripper gas we used Ar for several reasons: no background reactions initiated at the relevant energies, large probability of high ^{16}O charge states compared to lighter gases such as Ne, and easy and cheap access. From similar previous work [18] one expects an equilibrium charge state distribution for ^{16}O ions of several MeV at an Ar density of about 4×10^{16} atoms/cm^2. As discussed below, this expectation was essentially verified and we also found no significant increase in background in the spectra of the telescope, i.e. no ^{16}O events were observed due to Ar gas filled into the post-stripper cell.

Similar as in the case of ^{4}He gas, we measured the charge-state curves of ^{16}O ions in Ar gas filled into the post-stripper cell as a function of gas flow through the cell. An example is illustrated in Fig. 4 for a 4^+ ^{16}O beam of $E_{lab} = 9.40$ MeV: the data show that an equilibrium charge state distribution is reached at a gas flow above 10 mbarl/s corresponding to a density of $n_{Ar} = 5.6 \pm 0.6 \times 10^{16}$ atoms/cm^2 (Section 5). Measurements with different incoming charge states of the ^{16}O ions at a given energy led to the same probabilities for the equilibrium charge states within experimental uncertainty. The resulting equilibrium charge state probabilities as a function of ^{16}O energy are shown in Fig. 5.

We checked the consistency of the above results at $E = 2.7$ MeV and for the selected charge state $q(^{16}O) = 6^+$ by observing the ^{16}O capture rate in the telescope (for 4.0 mbar ^{4}He pressure) as a function of Ar flow rate: Fig. 6 demonstrates the same rate within experimental uncertainty.

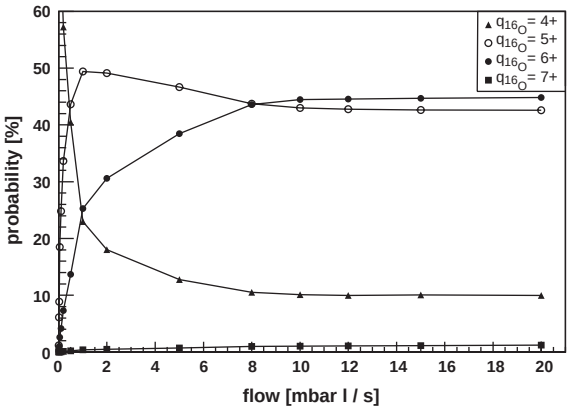

Fig. 4. Charge state distribution of ^{16}O ions in Ar gas ($q_{in} = 4^+, E_{lab} = 9.4$ MeV) as a function of Ar gas flow in the post-stripper cell; at low pressure the 4^+ charge state probability reaches 99.1% (not shown). The curves through the data points are to guide the eye.

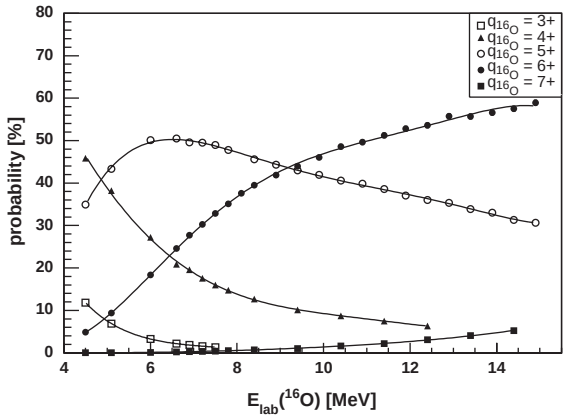

Fig. 5. Energy dependence of equilibrium charge states for ^{16}O ions in Ar gas. The curves through the data points are to guide the eye.

5. Gas target densities

The density of the stripper gas was measured via the energy loss of an ^{14}N beam at $E_{lab} = 2.0$ MeV, where the energy loss was observed using the 60° dipole magnet in connection with a current measurement at FC4: the procedure was described

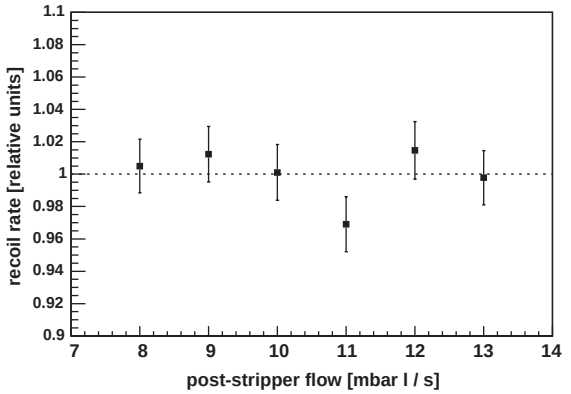

Fig. 6. Rate of ^{16}O recoils from ^{4}He(^{12}C,γ)^{16}O as a function of Ar flow rate in the post-stripper cell (for 4.0 mbar ^{4}He pressure): the horizontal line assumes no dependence.

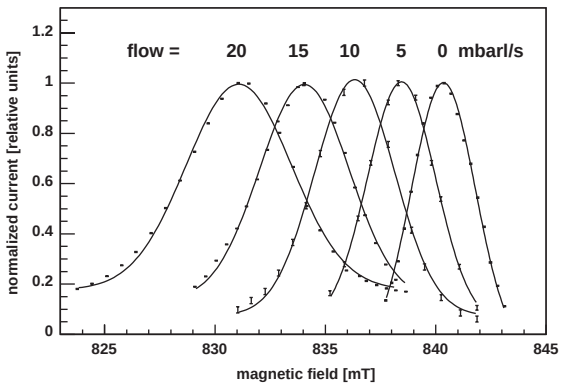

Fig. 7. Energy loss of a 2.0 MeV ^{14}N ion beam in Ar gas at flows of 0, 5, 10, 15, and 20 mbarl/s as observed with the 60° dipole magnet in connection with the current measurement at FC4, leading to magnetic field strengths of $B = 840.35$, 838.45, 836.39, 834.14, and 831.18 mT, respectively. The curves through the data points are Gaussian fits.

previously [16]. The results for an Ar gas flow of 0, 5, 10, 15, and 20 mbarl/s are shown in Fig. 7: for a flow of 10 mbarl/s one finds a shift in the magnetic field (compared to zero flow) of $\Delta B = 3.96 \pm 0.05$ mT, which in turn corresponds to an energy loss of $\Delta E = 18.8 \pm 0.2$ keV. Using stopping powers from SRIM2003 [19] (with an assumed 10% error) one arrives at the Ar density quoted above. For an Ar gas flow of 5, 15, and 20 mbarl/s one finds $n_{Ar} = 2.7 \pm 0.3$, 8.8 ± 0.9, and 13.0 ± 1.3 (10^{16}atoms/cm^2), respectively.

For the determination of the ^{4}He density in the primary gas target we used previously [16] the $E_{R,lab} = 1.668$ MeV resonance in ^{4}He(^{7}Li,γ)^{11}B at a pressure of 4.0 mbar to arrive at $n_{^4He} = (4.2 \pm 0.5) \times 10^{17}$ atoms/cm^2. The result was tested [16] via the energy loss of a ^{14}N beam at $E_{lab} = 2.0$ MeV, where the energy loss was again observed using the 60° dipole magnet in connection with a current measurement at FC4: $n_{^4He} = (4.7 \pm 0.5) \times 10^{17}$ atoms/cm^2. In the present work, we continued the energy loss measurements using the 60° dipole magnet for ^{7}Li ions ($E_{lab} = 1.7$ MeV), ^{14}N ions ($E_{lab} = 2.0$ MeV), and ^{12}C ions ($E_{lab} = 9.6$ MeV) leading to $n_{^4He} = 4.49 \pm 0.45, 4.49 \pm 0.45$, and 3.97 ± 0.40 (10^{17} atoms/cm^2), where the quoted error arises predominantly from an assumed 10% uncertainty in the stopping power. For the ^{14}N data we used the energy loss data reported by [21], while the energy loss data for ^{7}Li and ^{12}C ions were based on SRIM2003.

The elastic scattering yield was observed with 2 Si detectors ($\vartheta_{lab} = 75°$) placed within the ^{4}He gas cell and one Si detector ($\vartheta_{lab} = 60°$) placed between the gas cell and the post-stripper cell at two different positions along the beam axis. For 4.0 mbar ^{4}He gas and an Ar flow of 10 mbarl/s the 2 Si detectors showed no Ar gas inside the ^{4}He gas cell (Ar/He < 0.01%). The other Si detector indicated a mutual blocking of both gas flows in the region between the two gas cells, i.e. the He and Ar gases do not mix and their densities (quoted above) remain essentially unchanged in the gas combination.

6. Beam heating of the gas target

Previous studies have shown [20] that the density in an extended gas target can be significantly reduced due to heating effects of the ion beam along the beam axis. The effect depends on gas pressure, beam current, beam diameter, and energy loss. For the parameters of the present work (4.0 mbar He pressure, 20 pμA ^{12}C beam current, 3 mm beam diameter) one expects a negligible heating effect (<1%). We tested this expectation at a pressure of 4.0 mbar and a ^{12}C

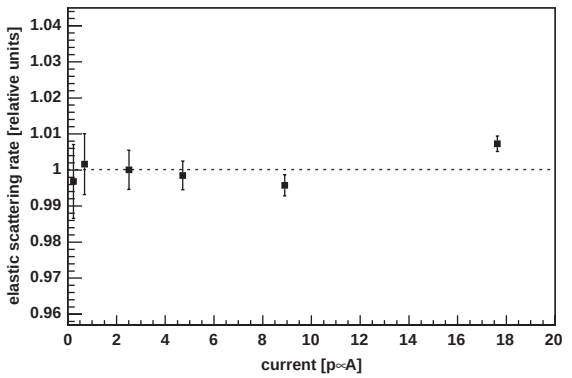

Fig. 8. The $^{12}C+^{4}He$ elastic scattering yield (for $E_{lab} = 9.6\,MeV$ and $p(^{4}He) = 4.0\,mbar$) observed with one of the 2 Si detectors in the gas cell is shown as a function of ^{12}C beam current: the horizontal line assumes no beam heating effects (note the suppressed scale of the ordinate). The results for the other Si detector are similar.

beam of $E_{lab} = 9.6\,MeV$ as a function of ^{12}C beam current as measured at FC2 (without gas). The chosen energy corresponds to the maximum of the energy loss curve. The target density was monitored via the $^{12}C+^{4}He$ elastic scattering yield observed in the 2 Si detectors placed inside the gas cell at $\vartheta_{lab} = 75^{\circ}$ on both sides of the beam axis. The results are shown in Fig. 8: the elastic scattering yield is independent of beam current and thus no beam heating effect exists in the present work, as expected.

7. Acceptance of the separator along the extended gas target

The observed pressure profile of the gas target (observed length FWHM = 38 mm) extended with its tails outside the gas cell over a total length of about 80 mm [16]. Calculations indicated a consequent reduction in acceptance at the extreme ends of the pressure profile. Averaged over the pressure profile one expected an acceptance of about 99.1% and 99.7% at $E = 1.3$ and 4.5 MeV, respectively, for a constant cross section along the target. To test these calculations, we investigated the acceptance along the beam axis covering the locations of the tails of the pressure profile. For this purpose, the gas cell was replaced by a set of scanning plates, which could in situ be rotated around the beam axis (for horizontal and vertical scanning) as well as be moved along the beam axis (over a distance of about 40 mm on the upstream and downstream side of the gas cell). The procedure was identical to that described previously [15]. Briefly, a voltage U applied to the plates (gap $d = 14\,mm$, length $L = 200\,mm$, width = 30 mm) led to an angular deflection of the ^{16}O projectiles of energy E_{lab} and charge state q in the amount of $\vartheta = \arctan(qUL/2E_{lab}d)$ simulating the emission cone of the ^{16}O recoils produced in $^{4}He(^{12}C,\gamma)^{16}O$ at the target position corresponding to the middle point of the plates.

In the first step, the plates were placed at the center of the gas target cell. After a proper setting of the separator, the angular acceptance was measured both for horizontal and vertical deflections. In the second step, the plates were moved upstream from the gas cell position by 40 mm (leaving the separator unchanged) and the angular acceptances were measured. Finally, the plates were moved downstream from the gas cell position by 40 mm (leaving the separator again unchanged) with a subsequent measurement of the angular acceptances. The results obtained at $E_{lab}(^{16}O) = 3.9\,MeV$ ($E = 1.3\,MeV$) are shown in Fig. 9: a 100% acceptance over an angular range larger than needed has been found at all positions. Similar results have been found at energies up to $E = 5.0\,MeV$; when the observed acceptances have not been fully satisfying, a slight retuning of the separator was performed. The data confirm the beam optical predictions.

8. Conclusions

The present work illustrates the need of a post-stripper cell to arrive at reliable charge state information for the ^{16}O recoils: the observations are of general importance for any recoil separator used in absolute cross section measurements. We also demonstrated that the angle and energy acceptances of the ERNA separator are well fulfilled also along the extended gas target cell.

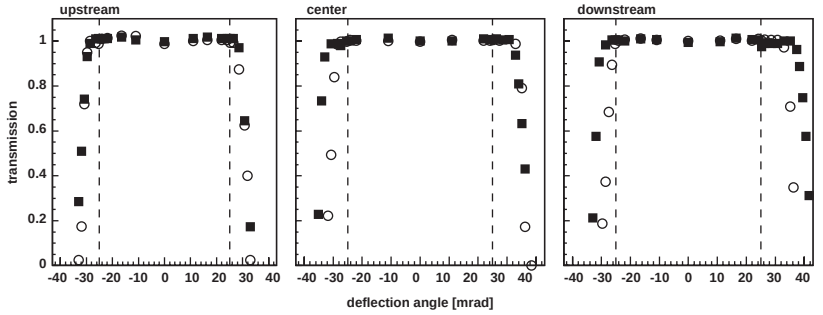

Fig. 9. Angle acceptances at $E_{lab}(^{16}O) = 3.9$ MeV ($E = 1.3$ MeV) in horizontal (full squares) and vertical (open circles) planes with the deflection plates located at the position of the gas cell (“center”), 40 mm upstream and 40 mm downstream from the gas cell position. The needed acceptances for the measurement of $^{4}He(^{12}C,\gamma)^{16}O$ are indicated by dashed lines.

References

[1] C. Rolfs, W.S. Rodney, Cauldrons in the Cosmos, University of Chicago Press, Chicago, 1988.
[2] G. Imbriani, M. Limongi, L. Gialanella, F. Terrasi, O. Straniero, A. Chieffi, Astrophy. J. 558 (2001) 903.
[3] O. Straniero, I. Dominguez, G. Imbriani, L. Piersanti, Astrophy. J. 583 (2003) 878.
[4] P. Dyer, C.A. Barnes, Nucl. Phys. A 233 (1974) 495.
[5] K.U. Kettner, H.W. Becker, L. Buchmann, J. Görres, H. Kräwinkel, C. Rolfs, P. Schmalbrock, H.P. Trautvetter, A. Vlieks, Z Phys. A 308 (1982) 73.
[6] A. Redder, H.W. Becker, C. Rolfs, H.P. Trautvetter, T.R. Donoghue, T.C. Rinkel, J.W. Hammer, K. Langanke, Nucl. Phys. A 462 (1987) 385.
[7] R.M. Kremer, C.A. Barnes, K.H. Chang, H.C. Evans, B.W. Filippone, K.H. Hahn, L.W. Mitchell, Phys. Rev. Lett. 60 (1988) 1475.
[8] J.M.L. Ouellet, H.C. Evans, H.W. Lee, J.R. Leslie, J.D. MacArthur, W. McLatchie, H.B. Mak, P. Skensved, J.L. Witton, X. Zahao, T.K. Alexander, Phys. Rev. C 54 (1996) 1982.
[9] G. Roters, C. Rolfs, F. Strieder, H.P. Trautvetter, Eur. Phys. J. A 6 (1999) 451.
[10] D. Rogalla, Diplomarbeit, Ruhr-Universität Bochum (1997).
[11] L. Gialanella, et al., Eur. Phys. J. A 11 (2001) 357.
[12] R. Kunz, M. Fey, M. Jaeger, A. Mayer, J.W. Hammer, G. Staudt, S. Harissopulos, T. Paradellis, Astron. J. 567 (2002) 643.
[13] D. Rogalla, et al., Nucl. Instr. and Meth. A 437 (1999) 266.
[14] D. Rogalla, et al., Eur. Phys. J. A6 (1999) 471.
[15] D. Rogalla, et al., Nucl. Instr. and Meth. A 513 (2003) 573.
[16] L. Gialanella, et al., Nucl. Instr. and Meth. A 522 (2004) 432.
[17] B. Cijek, I. Hunyadi, I.M. Szöghy, Phys. Rev. C 39 (1989) 1326.
[18] W. Liu, et al., Nucl. Instr. and Meth. A 496 (2003) 198.
[19] J.P. Biersack, J.F. Ziegler, Transport of Ions in Matter, TRIM program Version 2003, IBM Research, New York, 1995.
[20] J. Görres, K.U. Kettner, H. Kräwnkel, C. Rolfs, Nucl. Instr. and Meth. 177 (1980) 295.
[21] J.L. Price, D.G. Simons, S.H. Stern, D.J. Land, N.A. Guardala, J.G. Brennan, M.F. Stumborg, Phys. Rev. A 47 (1993) 2913.